Chapter 16

BG Model Based on Bagnold's Concept and Its Application to Analysis of Elongation of Sand Spit and Shore – Normal Sand Bar

Takaaki Uda, Masumi Serizawa and Shiho Miyahara

Additional information is available at the end of the chapter

http://dx.doi.org/10.5772/48547

1. Introduction

The accurate prediction of three-dimensional (3D) beach changes on a coast with a large shoreline curvature, such as a coast with a sand spit, and a wave field that significantly changes in response to topographic changes, has been difficult to achieve in previous studies. As a result, regarding the beach changes around a sand spit, most previous studies have focused on the shoreline changes. Ashton et al. (2001) showed that when the incident angle of deep-water waves to the mean shoreline exceeds 45°, shoreline instability occurs, resulting in the development of sand spits from a small perturbation of the shoreline. They successfully predicted the planar changes in a shoreline containing sand spits using infinitesimal meshes divided in the x- and y-directions. However in Ashton et al.'s model, only the longshore sand transport equation is employed as the sand transport equation instead of a two-dimensional (2D) sand transport equation in which both cross-shore and longshore sand transport are considered. Furthermore, in evaluating the wave field, wave conditions at the breaking point are transformed into deep-water values assuming a bathymetry with straight parallel contours and using Snell's law. Since the sand transport equation is expressed using these deep-water parameters, the effect of large 3D changes in topography on the wave field cannot be accurately evaluated. Furthermore, the finite-difference scheme used to evaluate the breaker angle and the method of calculating the wave field around the wave-shelter zone are altered depending on the calculation conditions, resulting in a complicated calculation method that requires special calculation techniques. Watanabe et al. (2004) developed a model for predicting the shoreline changes of a sand spit under the conditions that the sand spit significantly changes its configuration with changes in the wave field. They selected orthogonal curvilinear coordinates parallel and normal to the shoreline of the sand spit, and the seabed topography after various

numbers of time steps was inversely determined from the time-dependent shoreline configuration given by the seabed slope. They also predicted the shoreline changes due to the spatial changes in longshore sand transport. Their model is also not a definitive model for predicting the 3D topographic changes of a sand spit.

A sand spit is often formed by wave action at a location where the direction of the coastline abruptly changes. Uda & Yamamoto (1992) carried out a movable-bed experiment using a plane-wave basin to investigate the development of a sand spit. Two experiments were carried out: sand was deposited (1) on a shallow flat seabed and (2) on a coast with a steep slope. Their results showed that a slender sand spit extends along the marginal line between the shallow sea and offshore steep slope in Case 1, whereas a cuspate foreland is formed owing to the deposition of sand on the steep slope in Case 2, suggesting the importance of the effect caused by the difference in the depth of water where sand is deposited. We have developed a model for predicting beach changes based on Bagnold's concept (Serizawa et al., 2006) by applying the concept of the equilibrium slope introduced by Inman& Bagnold (1963) and the energetics approach of Bagnold (1963). Here, the BG model is used to simulate the extension of a sand spit on a shallow seabed and the formation of a cuspate foreland on a steep coast (Serizawa & Uda, 2011).

As another type of beach change due to waves on a coast with a shallow flat seabed, a tidal flat facing an inland sea is considered. On such a tidal flat subject to the action of waves with significant energy, a sandy beach may develop along the marginal line between the tidal flat and the land, and the sandy beach with a steep slope is clearly separated from the tidal flat along a line with a discontinuous change in the slope. On such beaches developing along the marginal line between the tidal flat and the land, longshore sand transport due to the oblique wave incidence to the shoreline and cross-shore sand transport during storm surges often occur. However, in addition to these sand transport phenomena, as part of the interaction between the tidal flat and the sandy beach, shoreward transport and the landward deposition of sand originally supplied from the offshore zone of the tidal flat, forming a slender sand bar, are often observed. Although this landward sand movement due to waves on the shallow tidal flat is considered to be part of the process by which sand transported offshore by river currents during floods returns to the shore, its mechanism has not yet been studied. These phenomena were observed on the Kutsuo coast, which has a very wide tidal flat and faces the Suo-nada Sea, part of the Seto Inland Sea, Japan. Here, the BG model was also used to predict the extension of a slender shore-normal sand bar observed on this coast (Serizawa et al., 2011). The observed phenomena were successfully explained by the results of the numerical simulation.

2. Numerical model (BG model)

With the elongation of a sand spit or a sand bar, the shape of the wave-shelter zone behind the spit or the sand bar changes, and therefore, the repeated calculation of the wave field and topographic changes is required. We use Cartesian coordinates (x, y) and consider the elevation at a point Z (x, y, t) as a variable to be solved, where t is time. The beach changes

are assumed to take place between the depth of closure h_c and the berm height h_R. A modified version of the BG model proposed by Serizawa et al. (2009a) was used to predict the formation of a sand spit. An additional term given by Ozasa & Brampton (1980) was also incorporated into the fundamental equation of the BG model to accurately evaluate the longshore sand transport due to the effect of the longshore gradient of the wave height. The fundamental equation is given by

$$\vec{q} = C_0 \frac{P}{\tan\beta_c} \left\{ \begin{array}{l} K_n \left(\tan\beta_c \vec{e_w} - |\cos\alpha| \ \vec{\nabla Z} \right) \\ + \left\{ \left(K_s - K_n \right) \sin\alpha - \dfrac{K_2}{\tan\bar{\beta}} \dfrac{\partial H}{\partial s} \right\} \tan\beta \vec{e_s} \end{array} \right\} \quad \left(-h_c \le Z \le h_R \right) \tag{1}$$

$$P = \rho \, u_m^3 \tag{2}$$

$$u_m = \frac{H}{2} \sqrt{\frac{g}{h}} \tag{3}$$

Here, $\vec{q} = \left(q_x, q_y \right)$ is the net sand transport flux, Z (x, y, t) is the elevation, n and s are the local coordinates taken along the directions normal (shoreward) and parallel to the contour lines, respectively, $\vec{\nabla Z} = \left(\partial Z / \partial x, \ \partial Z / \partial y \right)$ is the slope vector, $\vec{e_w}$ is a unit vector in the wave direction, $\vec{e_s}$ is a unit vector parallel to the contour lines, α is the angle between the wave direction and the direction normal to the contour lines, $\tan\beta = \left| \vec{\nabla Z} \right|$ is the seabed slope, $\tan\beta_c$ is the equilibrium slope, $\tan\beta \ \vec{e_s} = \left(-\partial Z / \partial y, \ \partial Z / \partial x \right)$, K_s and K_n are the coefficients of longshore sand transport and cross-shore sand transport, respectively, K_2 is the coefficient of the term given by Ozasa & Brampton (1980), $\partial H / \partial s = \vec{e_s} \cdot \vec{\nabla H}$ is the longshore gradient of the wave height H measured parallel to the contour lines and $\tan\bar{\beta}$ is the characteristic slope of the breaker zone. In addition, C_0 is the coefficient transforming the immersed-weight expression into a volumetric expression ($C_0 = 1 / \left\{ \left(\rho_s - \rho \right) g \left(1 - p \right) \right\}$, where ρ is the density of seawater, ρ_s is the specific gravity of sand particles, p is the porosity of sand and g is the acceleration due to gravity), u_m is the amplitude of the seabed velocity due to the orbital motion of waves given by Eq. (3), h_c is the depth of closure, and h_R is the berm height.

The intensity of sand transport P in Eq. (1) is assumed to be proportional to the wave energy dissipation rate ϕ based on the energetics approach of Bagnold (1963). In the model of Serizawa et al. (2006), P was formulated using the wave energy at the breaking point, but in this study, it is combined with the wave characteristics at a local point. Bailard & Inman (1981) used the relationship $\phi_t = \tau u_t = \rho C_f u_t^3$ for the instantaneous wave energy dissipation rate ϕ_t to derive their sand transport equation, where τ is the bottom shear stress, u_t is the instantaneous velocity and C_f is the drag coefficient. We basically follow their study but assume that ϕ is proportional to the third power of the amplitude of the bottom oscillatory velocity u_m due to waves instead of the third power of the instantaneous velocity. The intensity of sand transport P is then given by Eq. (2), and its coefficient is assumed to be

included in the coefficients of longshore and cross-shore sand transport, K_s and K_n, respectively. u_m can be calculated by small-amplitude wave theory in shallow water using the wave height H at a local point (Eq. (3)), which can be obtained by the numerical calculation of the plane-wave field. The depth of closure h_c is assumed to be proportional to the wave height H at a local point and is given by Eq. (4), referring to the relationship given by Uda & Kawano (1996).

$$h_c = KH \qquad (K=2.5) \tag{4}$$

In the numerical simulation of beach changes, the sand transport equation and the continuity equation are solved on the x-y plane by the explicit finite-difference methodemploying staggered mesh scheme. In the estimation of sand transport near the berm top and the depth of closure, sand transport was linearly reduced to 0 near the berm height or the depth of closure to prevent sand from depositing in the area higher than the berm height and beach erosion in the zone deeper than the depth of closure.

The wave field was calculated using the energy balance equation given by Mase (2001), in which the directional spectrum D (f, θ) of the irregular waves varies with the energy dissipation term due to wave breaking (Dally et al., 1984). Here, f and θ are the frequency and wave direction, respectively. In this method, wave refraction, wave breaking and wave diffraction in the wave-shelter zone can be calculated with a small calculation load. The energy dissipation term due to wave breaking ϕ (Dally et al., 1984), which is incorporated into the energy balance equation (Eq. (5)), is given by

$$\frac{\partial}{\partial x}\left(DV_x\right)+\frac{\partial}{\partial y}\left(DV_y\right)+\frac{\partial}{\partial \theta}\left(DV_\theta\right)=F-\phi \tag{5}$$

$$\phi=\left(K/h\right)DC_g\left[1-\left(\Gamma/\gamma\right)^2\right] \qquad \left(\phi\geq 0\right) \tag{6}$$

Here, D is the directional spectrum, (V_x, V_y, V_θ) is the energy transport velocity in the (x, y, θ) space, F is the wave diffraction term given by Mase (2001), K is the coefficient of the wave-breaking intensity, h is the water depth, C_g is the wave group velocity ($C_g \approx \sqrt{gh}$ in the approximation in shallow-water wave theory), Γ is the ratio of the critical breaker height to the water depth on the horizontal bed and γ is the ratio of the wave height to water depth. To prevent the location where the berm develops from being excessively seaward compared with that observed in the experiment or the field, a lower limit was considered for h in Eq. (6). As a result of this procedure, wave decay near the berm top was reduced, resulting in a higher landward sand transport rate. In the calculation of the wave field on land, the imaginary depth h' between the minimum depth h_0 and berm height h_R was considered, as given by Eq. (7), similarly to in the ordinary 3D model (Shimizu et al., 1996).

$$h'=\left(\frac{h_R-Z}{h_R+h_0}\right)^r h_0 \qquad \left(r=1\right) \qquad \left(-h_0\leq Z\leq h_R\right) \tag{7}$$

In addition, at locations whose elevation is higher than the berm height, the wave energy was set to 0. The calculation of the wave field was carried out every 10 steps in the calculation of topographic changes.

Equation (1) shows that the sand transport flux can be expressed as the sum of the component along the wave direction and the components due to the effect of gravity normal to the contours and the effect of longshore currents parallel to the contours. To investigate the physical meaning of Eq. (1), $\vec{q}$ in Eq. (1) is separately expressed as Eq. (8) when neglecting the additional term given by Ozasa & Brampton (1980), and when the inner products of $\vec{e_n}$ and $\vec{q}$ and of $\vec{e_s}$ and $\vec{q}$ are taken, Eqs. (9) and (10) are derived for the cross-shore and longshore components of sand transport, q_n and q_s, respectively. Furthermore, under the condition that the seabed slope is equal to the equilibrium slope, Eq. (10) reduces to Eq. (11).

$$\vec{q} = q_n \vec{e_n} + q_s \vec{e_s} \tag{8}$$

$$q_n = \vec{e_n} \cdot \vec{q} = C_0 K_n P \left|\cos\alpha\right| \left(\frac{\cos\alpha}{\left|\cos\alpha\right|} - \frac{\tan\beta}{\tan\beta_c} \right) \tag{9}$$

$$q_s = \vec{e_s} \cdot \vec{q} = C_0 K_s P \sin\alpha \left\{ \frac{\tan\beta}{\tan\beta_c} + \frac{K_n}{K_s} \left(1 - \frac{\tan\beta}{\tan\beta_c} \right) \right\} \tag{10}$$

$$q_s \approx C_0 K_s P \sin\alpha \qquad \left(\because \tan\beta \approx \tan\beta_c \right) \tag{11}$$

In Eq. (9), the cross-shore sand transport q_n becomes 0 when the local seabed slope is equal to the equilibrium slope, and the longshore sand transport q_s becomes 0 when the wave direction coincides with the normal to the contour lines, as shown in Eqs. (10) and (11). When a discrepancy from these conditions arises, sand transport is generated by the same stabilization mechanism as in the contour-line-change model (Uda & Serizawa, 2010).

Taking the above into account, the first term in the parentheses in Eq. (1) gives the sand transport in the case that the rates of longshore and cross-shore sand transport are equal ($K_s = K_n$), and the second term is the additional longshore sand transport in the case that the rates are different ($K_s > K_n$). The physical meaning of the second term is that longshore sand transport is generated by the small angular shift that occurs when the wave direction is incompletely reversed in the oscillatory movement due to waves, and the second term also models the additional longshore sand transport due to the effect of longshore currents, the effect of which is only partially included in the first term.

Although the applicability of the contour-line-change model to the prediction of beach changes is limited when the shape of coastal structures is complicated because it tracks the movement of lines with specific characteristics, the BG model can be applied to the

prediction of topographic changes under all structural conditions, because the depth changes in the x-y plane are calculated, similarly to in the ordinary model for predicting 3D beach changes, and therefore the calculation can be carried out systematically. This is an advantage of the BG model.

3. Movable-bed experiment on elongation of a sand spit

A movable-bed experiment was carried out using a plane-wave tank of 16 m width and 21 m length (Uda & Yamamoto, 1992). A model beach was made of sand with d_{50} = 0.28 mm. A sandy beach was established as the source of sand in the right half of the plane basin and conditions were set up such that leftward longshore sand transport developed. In Case 1, a shallow seabed with a water depth of 5 cm was formed in the left half of the wave basin and an offshore bed was formed with a steep slope of 1/5. In Case 2, a steep slope of 1/5 was produced instead of a shallow sea where the sand spit was formed. The angle between the direction normal to initial shoreline and the wave direction was 20° in order for sufficient longshore sand transport to occur. The elevation of the flat surface on the land was assumed to be 10 cm above mean sea level. Regular waves with H_0' = 4.6 cm and T = 1.27 s incident to the model beach were generated for 8 hr. When a shallow sea exists, incident waves break immediately offshore of the shallow seabed, resulting in the rapid decay of waves on the shallow seabed. Because of this effect, sand is deposited near the marginal line between the shallow flat seabed and the steep offshore slope, resulting in the rapid elongation of a sand spit.

Figures 1(a)-1(c) show the initial bathymetry and the beach topography after wave generation for 1 and 8 hr in Case 1, respectively. Here, the arrows in Figs. 1(a) and 1(d) show the breaking point (the tip of the arrows), the breaker height (the length of the arrows), and the wave directionat the breaking point (the direction of the arrows) measured immediately after the start of wave generation. Because the shoreline had a discontinuity due to a sudden change in the shoreline direction between the sand supply zone and the shallow seabedwhere sand was deposited, a straight sand spit extended from the boundary, and a slender sand spit extended along the marginal line between the shallow seabed and the steepoffshore slope over time. After 8 hr, the sand spit had reached the left boundary while forming a barrier island, and the width of the barrier island expanded upcoast from the left boundary because of the continuous sand supply.

Figures 1(d) and 1(e) show the initial bathymetry and the beach topography after wave generation for 8 hr in Case 2 with a steep offshore slope. The water depth in the zone where sand was deposited was large; thus, sand was deposited while forming a steep slope.

Because this steep slope reaches a great depth, a cuspate foreland was formed without the development of a sand spit. These experimental results were used for validating the improved BG model.

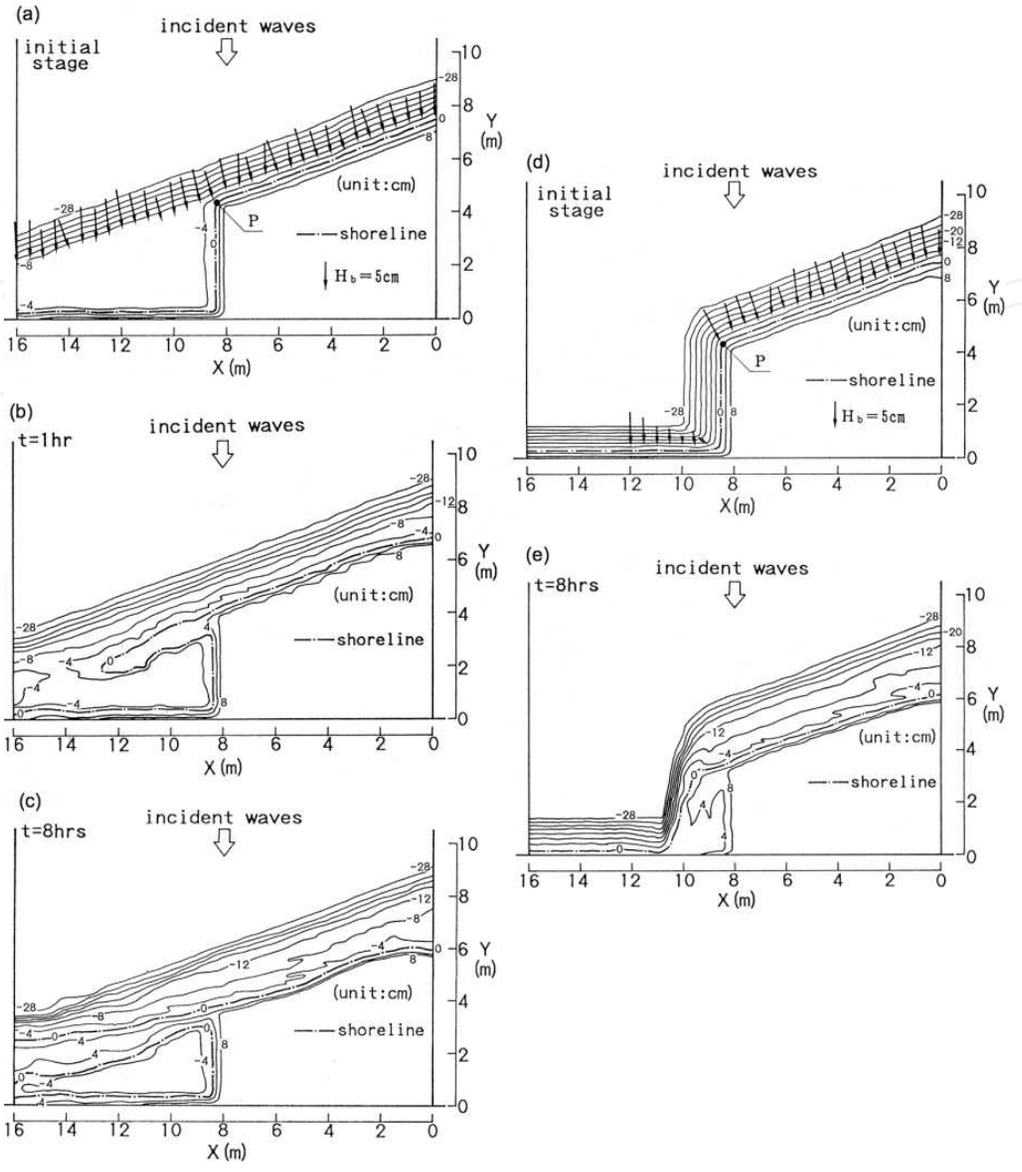

Figure 1. Experimental results for development of sand spit on a coast with abrupt change in coastline orientation (Uda & Yamamoto, 1992).

4. Field observation of formation of slender shore-normal sand bar

4.1. General conditions

The study area is the Kutsuo coast facing the Suo-nada Sea, part of the Seto Inland Sea, as shown in Fig. 2. Figure 3 shows an aerial photograph of the study area taken in 1999. The Harai River flows into the coast, which has a very wide tidal flat of approximately 1.5 km width offshore of the river. Although a river mouth bar extends on the north side of the Harai River, another slender sand bar has developed along the north side of the channel extending between the river mouth and the offshore tidal mud flat, and it intersects the river mouth bar perpendicular to the shoreline. The sand source for this slender sand bar is assumed to be the Harai River; sand transported offshore by flood currents is deposited

along both sides of the channel, and is then transported shoreward owing to the wave action.In this area, the slender sand bar as shown in Fig. 3 has been continuously developing. Figure 4 shows the bathymetry around the slender sand bar relative to the reference level (0.1m below mean sealevel) in 2008. Although the slender sand bar has moved slightly north compared with its position in Fig. 3, it extends in the cross-shore direction at X = 120 m in the central part of the river mouth bar, and the shoreline slightly protrudes near the connection point. The foreshore has been developing in the zone with elevation between 1.0 and 3.0 m. This foreshore is composed of coarse and medium-size sand, and its slope is as steep as 1/10. A tidal flat extends in the offshore zone, the elevation of which is lower than 1.0 m. In addition, there is a difference in the elevation of the tidal flat on both sides of the slender sand bar extending in the cross-shore direction with the ground elevation on the south side slightly higher than that on the north side.

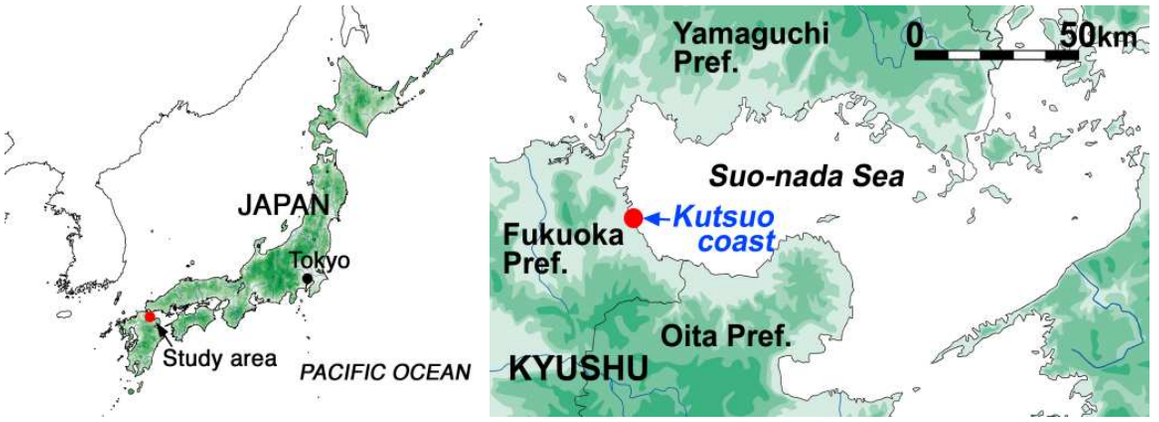

Figure 2. Location of Kutsuo coast facing Suo-nada Sea, part of Seto Inland Sea.

Figure 3. Aerial photograph of Kutsuo coast.

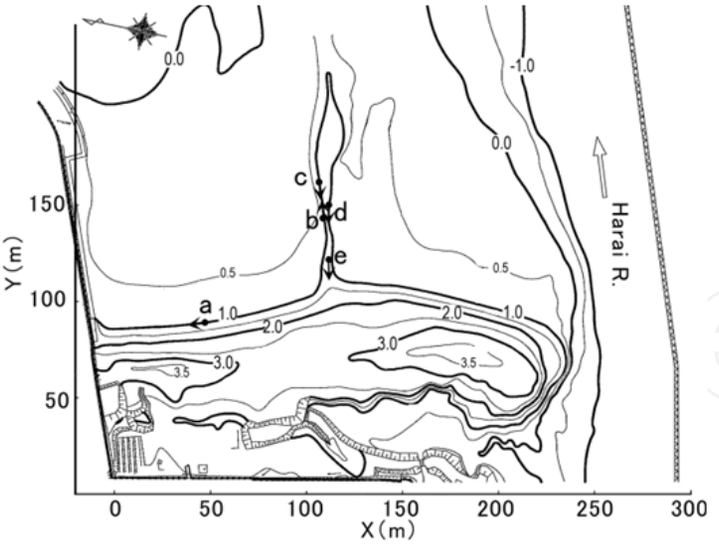

Figure 4. Bathymetry around slender sand bar on tidal flat offshore of Kutsuo coast.

4.2. Field observation

During low tide on December 27, 2009, a field observation of the tidal flat offshore of the coast was carried out. The north end of the coast is separated by a vertical seawall protecting a park, as shown in Fig. 5. A sandy beach abruptly begins with a steep slope from the mud flat covered by cohesive materials, and the mud flat and sandy beach are clearly separated along a line where the slope changes abruptly. The tidal flat is composed of cohesive materials, whereas the sandy beach is composed of coarse sand and is well compacted.

Figure 6 shows a view of the entire slender sand bar. Although the sand bar is submerged during high tide, it is completely exposed during low tide, as shown in Fig. 6. The sand bar extends in the direction normal to the mean coastline. Comparing the elevations of the mud flat on both sides of the sand bar, the elevation on the right (south) side, which is next to theoffshore channel, is higher than that on the left (north) side. On the south side of the slender sand bar, the Harai River flows into the sea, and sand supplied to the tidal flat from the river mouth is considered to be transported and deposited on the surface of the tidal flat owing to the shoreward sand transport due to waves. In this case, sand supply to the area north of the slender sand bar is obstructed by the sand bar itself, and this is assumed to be the cause of the difference in ground elevation on both sides of the sand bar.

Figure 7 shows the tip of a branch separated from the offshore part of the main slender sand bar, as shown in Fig. 3. On this sand bar, decomposed granite, which was considered to be transported offshore by flood currents of the river, has been deposited. The elevation of the sand bar gradually increases shoreward, then at the landward end suddenly drops to the tidal flat with a steep slope approximately equal to the angle of repose of the sand, implying the occurrence of shoreward sand transport.

Figure 8 shows the coastal conditions, looking landward from the tip of the slender sand bar. Although sand was deposited with a foreshore slope of 1/10 along the north side of the slender sand bar, the foreshore and flat tidal flat were clearly separated along the abrupt

Figure 5. Beach separated by vertical seawall (December 27, 2009).

Figure 6. View of entire slender sand bar (December 27, 2009).

change in the slope passing through point B. By a sieve analysis of the beach material sampled at point A, the median diameter of the beach material was determined to be d_{50} = 1.50 mm at point A. Figure 9 shows the narrow neck of the slender sand bar connected to the land. Several lines showing high tide marks extend in the cross-shore direction on the surface of the sand bar, implying that the sand bar stably exists during tidal changes. Figure 10 shows the beach condition near the point connecting the land and the slender sand bar. The triangular high tide lines show that the contour lines are parallel to these high tide lines. Therefore, if waves are incident from the direction normal to the coastline, large shoreward sand transport may occur along these contour lines because of the large incident wave angle. However, the slender sand bar is stable without rapid beach changes. Taking into account the continuity condition of sand and the fact that the slender sand bar is stable, the materials forming the sand bar are considered to have been carried from the Harai River during floods. The observation results indicate that the sand transported offshore by flood currents returns to the beach owing to shoreward sand transport due to waves. On an exposed beach, the formation of a stable sand bar extending normal to the coastline, as observed on this coast, is difficult, and such a sand bar rapidly deforms under wave action. Taking this into account, the formation of a slender sand bar observed in this study is

considered to be due to the typical sand movement observed on only a very shallow tidal flat.

Figure 7. Tip of branch separated from offshore part of main slender sand bar (December 27, 2009).

Figure 8. Coastal condition, while looking landward from tip of slender sand bar (December 27, 2009).

Figure 9. Narrow neck of slender sand bar connected to land (December 27, 2009).

Figure 10. Beach condition near point connecting land and slender sand bar (December 27, 2009).

5. Application to movable-bed experiment

At locations with elevations higher than the berm height, the wave energy was set to 0. For convenience, the space scale in the calculation was set to 100-fold that in the experiment, and then the calculated results were reduced 100-fold. Although the movable-bed experiment was carried out under regular wave conditions, the wave field was calculated using the energy balance equation for irregular waves while regarding regular waves in the experiment as irregular waves, because repeated calculations were necessary owing to the bathymetric changes in this calculation.

5.1. Formation of barrier island on flat shallow seabed

Given the same initial topography and wave conditions as those in the experiment (regular waves with H_0' = 4.6 cm and T = 1.27 s obliquely incident to the model beach with an angle of 20°), the beach changes after 8 hr were predicted. The depth of closure was given by h_c = 2.5H (H: wave height at a local point). The berm height was assumed to be 5 cm, and the angles of the equilibrium slope and repose slope were set as 1/5 and 1/2, respectively, on the basis of the experimental results. The calculation domain was divided by $\Delta x = \Delta y$ = 20 cm intervals in the cross-shore and longshore directions, respectively, and the calculation for up to 8 hr (8×10^4 steps) was carried out using time intervals of $\Delta t = 1\times10^{-3}$ hr. Table 1 shows the calculation conditions.

5.1.1. Bathymetric changes

Figures 11(a)-11(f) show the results for the predicted development of a sand spit on a shallow flat seabed given the same conditions as those in the experiment. A slender sand spit with a length of approximately 2 m was formed until 0.5 hr because of the deposition of sand supplied from upcoast along the marginal line between the flat shallow seabed and the steep offshore bottom, as shown in Fig. 11(b). Rapid shoreward sand transport also occurred owing to the restoration effect of the beach slope corresponding to the deviation from the

Wave conditions	Incident waves: H_I= 4.6 m (4.6 cm), T = 12.7 s (1.27 s), wave direction θ_I=20° relative to normal to initial shoreline
Berm height	h_R= 5 m (5 cm)
Depth of closure	h_c = 2.5H (H: wave height)
Equilibrium slope	tanβ_c=1/5
Angle of repose slope	tanβ_S=1/2
Coefficients of sand transport	Coefficient of longshore sand transport K_s=0.045 Coefficient of Ozasa & Brampton (1980) term K_2 = 1.62K_s Coefficient of cross-shore sand transport K_n = 0.1K_s
Mesh size	Δx = Δy = 20 m
Time intervals	Δt = 0.001 hr (0.01 hr)
Duration of calculation	80 hr (8×10^4 steps) (8 hr)
Boundary conditions	Shoreward and landward ends: q_x = 0, left and right boundaries: q_y = 0
Calculation of wave field	Energy balance equation (Mase, 2001) •Term of wave dissipation due to wave breaking: Dally et al. (1984) model •Wave spectrum of incident waves: directional wave spectrum density obtained by Goda (1985) •Total number of frequency components N_F = 1 and number of directional subdivisions N_θ= 8 •Directional spreading parameter S_{max} = 75 •Coefficient of wave breaking K = 0.17 and Γ= 0.3 •Imaginary depth between minimum depth h_0 and berm height h_R : h_0= 2 m (2 cm) •Wave energy = 0 where $Z \geq h_R$ •Lower limit of h in terms of wave decay due to breaking: 0.7 m (0.7 cm)
Remarks	Numbers in parentheses show experimental values. Space and time scales in the calculation are 100- and 10-fold those in the experiment, respectively.

Table 1. Calculation conditions (numbers in parentheses: experimental conditions).

equilibrium slope, because the seabed had an abrupt change in the slope along this marginal line along which sand was deposited, whereas the intervals between the contours became large in the offshore zone shallower than h_c. The sand spit further extended along the marginal line with increasing time, and the length of the spit reached 3.5 m after 1 hr, as shown in Fig. 11(c). After 2 hr, the tip of the spit was connected to the left boundary and a barrier island had formed, enclosing a lagoon behind the barrier island (Fig. 11(d)). Although a slender, straight sand spit extended along the marginal line until 2 hr after the start of wave generation, sand started to be deposited upcoast of the left boundary after 4 hr

because of the blockage of longshore sand transport by the left boundary. Offshore sand transport in the deep zone also occurred, as shown in Fig. 11(e). During this process, the shoreline advanced and the width of the barrier island formed by the extension of the sand spit gradually increased from the left boundary. After 8 hr, the effect of the blockage of longshore sand transport by the left boundary had reached the upcoast and the width of the barrier island had also increased at X = 9 m, where the sand spit first developed, as shown in Fig. 11(f).

We compared the experimental results after 1 hr with the calculated results, as shown in Figs. 1(b) and 11(c), respectively. Both sets of results indicated that a sand spit extended from the location with a sudden change in the coastline orientation along the marginal line on the flat shallow seabed and were in good agreement. However, there was some discrepancy in the location of the tip of the sand spit. Similarly, both experimental and calculated results after 8 hr, shown in Figs. 1(c) and 11(f), respectively, are in good agreement in that the width of the barrier island was increased by the blockage of longshore sand transport by the left boundary and that a gentle slope was formed at a depth of approximately 8 cm owing to erosion along with the formation of a scarp near the right boundary. With regard to the experimental results for the extension of the sand spit reported by Uda & Yamamoto (1992), Watanabe et al. (2004) successfully predicted the shoreline changes related to the extension of the sand spit using a one-line model with a curvilinear coordinate system. However, in the present study, we were able to predict the development of a barrier island after the extension of the sand spit.

Figures 12(a)-12(f) show bird's-eye view of the extension of the barrier island in Case 1, looking upcoast from above the downcoast. Although a simple sand spit extended from the boundary between the sand supply and accretion zones on the flat shallow seabed, sand had already been transported shoreward, forming a subsurface sand bar along the marginal line between the steep offshore slope and flat shallow seabed, until 0.5 hr before the extension of the sand spit, implying the generation of rapid shoreward sand transport at the abrupt change in the slope. Furthermore, sand was deposited over the steep offshore slope between 4 and 8 hr after the start of wave generation and an extremely steep slope was formed near the downcoast boundary. In contrast, a wave-cut gentle slope was formed offshore of the erosion zone located upcoast.

5.1.2. Changes in wave field

Significant changes in the wave field occurred on the shallow flat seabed with the extension of the barrier island, as shown in Fig. 13. Initially, the wave height was reduced by up to approximately 1.5 cm because of wave breaking along the marginal line of the shallow flat seabed. However, the extension of the sand spit owing to the shoreward sand transport was very rapid, and the wave height was markedly reduced on the shallow flat seabed after wave generation for 1 hr. After 8 hr, a calm wave zone extended in the entire area behind the barrier because of the rapid development of the barrier, and the wave height had a uniform distribution.

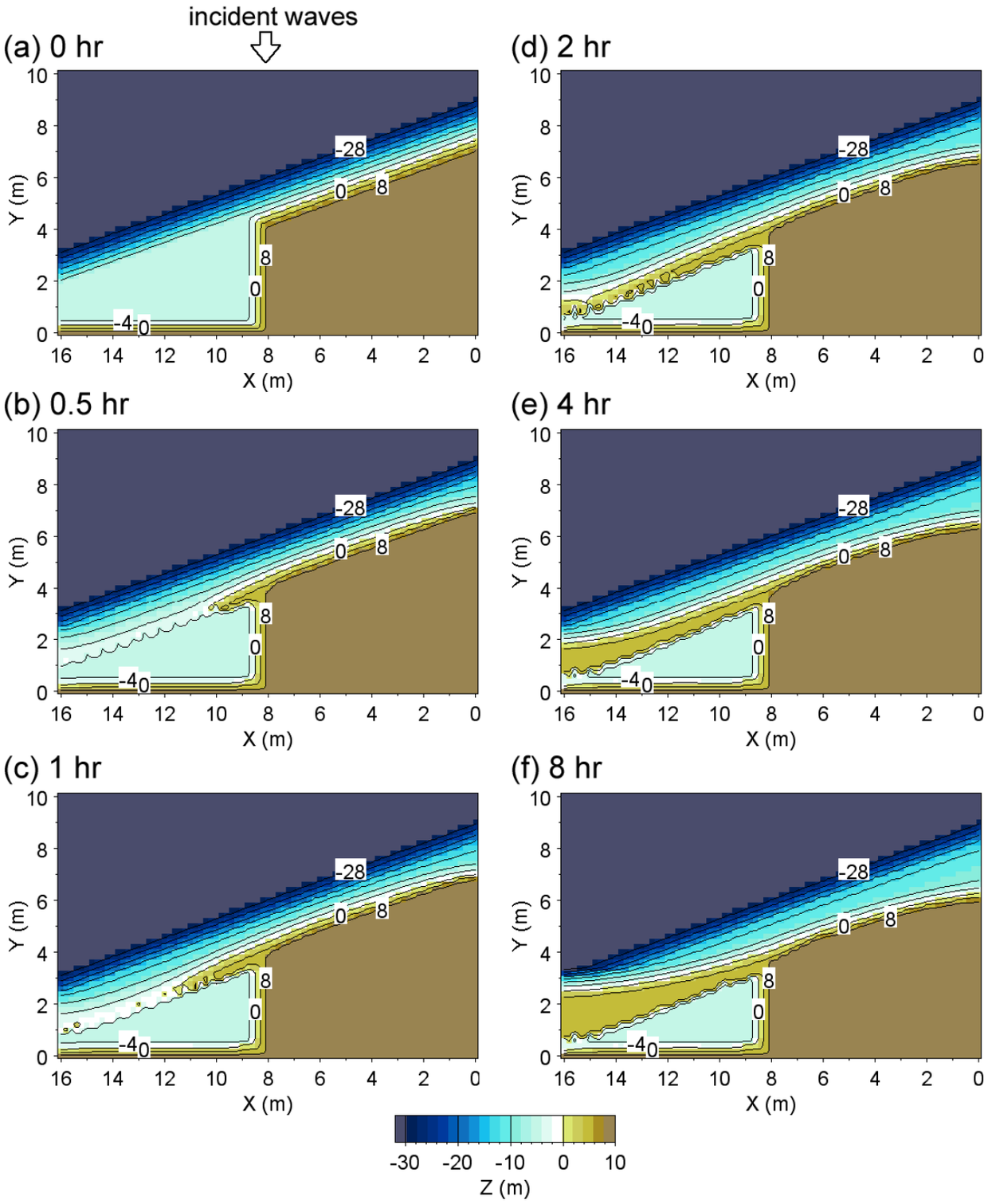

Figure 11. Results for predicted development of sand spit on a coast with abrupt change in coastline orientation (Case 1: flat shallow seabed).

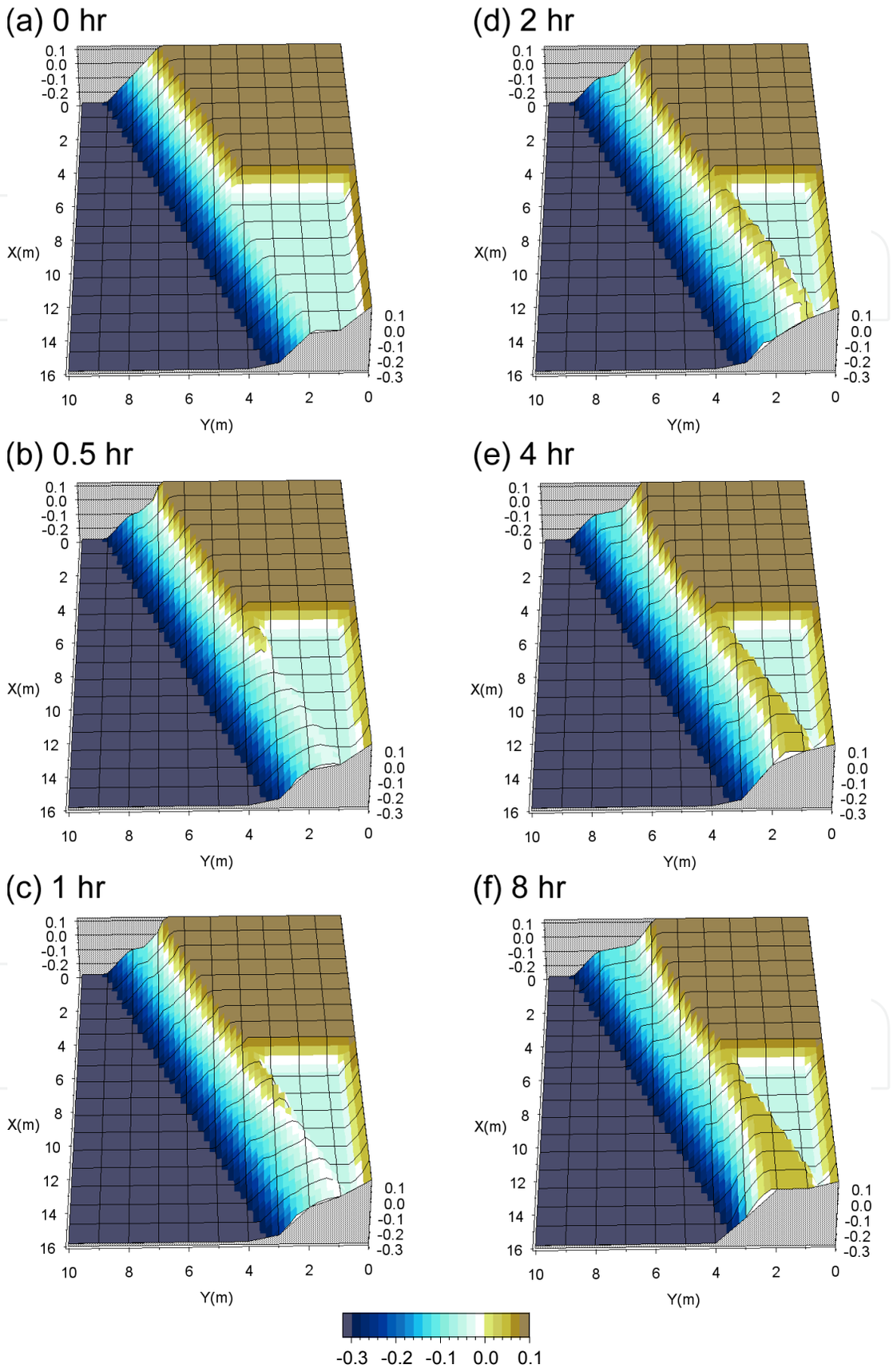

Figure 12. Bird's-eye view of topographic changes (Case 1: flat shallow seabed).

5.1.3. Sand transport flux

Figure 14 shows the sand transport flux 0, 1 and 8 hr after the start of wave generation. Although the initial sand transport flux was large in the area to the right of X = 8 m, where the sand source was located, the area with a large sand transport flux had moved left with the extension of the sand spit after 1 hr. In contrast, the sand transport flux decreased in magnitude near the right boundary, because the angle between the direction normal to the contour lines and the direction of incident waves was reduced. After 8 hr, the sand spit had reached the left boundary and the sand transport flux had significantly decreased, and the area with a large sand transport flux had become small.

5.1.4. Changes in longitudinal profiles

Figures 15(a)-15(d) show the experimental and predicted changes in longitudinal profiles along transect X = 0 m located at the right boundary, and transects X = 9, 12 and 14 m crossing the flat shallow seabed, respectively. Along transect X = 0 m, although the experimental and predicted results, which indicated that the depth of closure was -12 cm, are in agreement, as shown in Fig. 15(a), the eroded volume in the calculation was overestimated in the nearshore zone, where there was less scarp erosion. However, the sand budget in the cross section was approximately maintained and the parallel recession of the cross section while maintaining a constant slope was accurately predicted in the calculation. Along transect X = 9 m, the development of a berm of 5 cm height after 1 hr, as shown in Fig. 15(b), was observed in both the experiment and simulation, but the location of the berm was slightly seaward in the simulation. After 8 hr, however, the berm location had moved landward and a stable barrier island had formed. These experimental and calculated changes are in good agreement. Furthermore, no beach changes occurred on the flat shallow seabed because the elongation of the sand spit was too rapid to permit wave intrusion into the flat seabed. Along transect X = 12 m, the elongation of the sand spit was limited until 1 hr, as shown in Fig. 15(c), and there was little development of the berm. However, a substantial berm had developed after 8 hr. The experimental and calculated results are in good agreement regarding these points. Along transect X = 14 m near the left boundary, although a sand bar did not develop until 1 hr, a large amount of sand had been deposited after 8 hr, forming a barrier island with a 1.2 m width, as shown in Fig. 15(d). In this case, the seabed slope gradually steepened because of the continuous deposition of sand along the offshore steep slope, resulting in the deposition of sand up to a depth of -23 cm, which is approximately two fold larger than the depth of closure of -12 cm.

5.2. Formation of cuspate foreland on steep coast

5.2.1. Bathymetric changes

Figures 16(a)-16(f) show the results for the calculation of the development of a cuspate foreland on a steep coast t = 0, 0.5, 1, 2, 4, and 8 hr after the start of wave generation given the same conditions as those in the experiment. The contour lines that extended parallel to

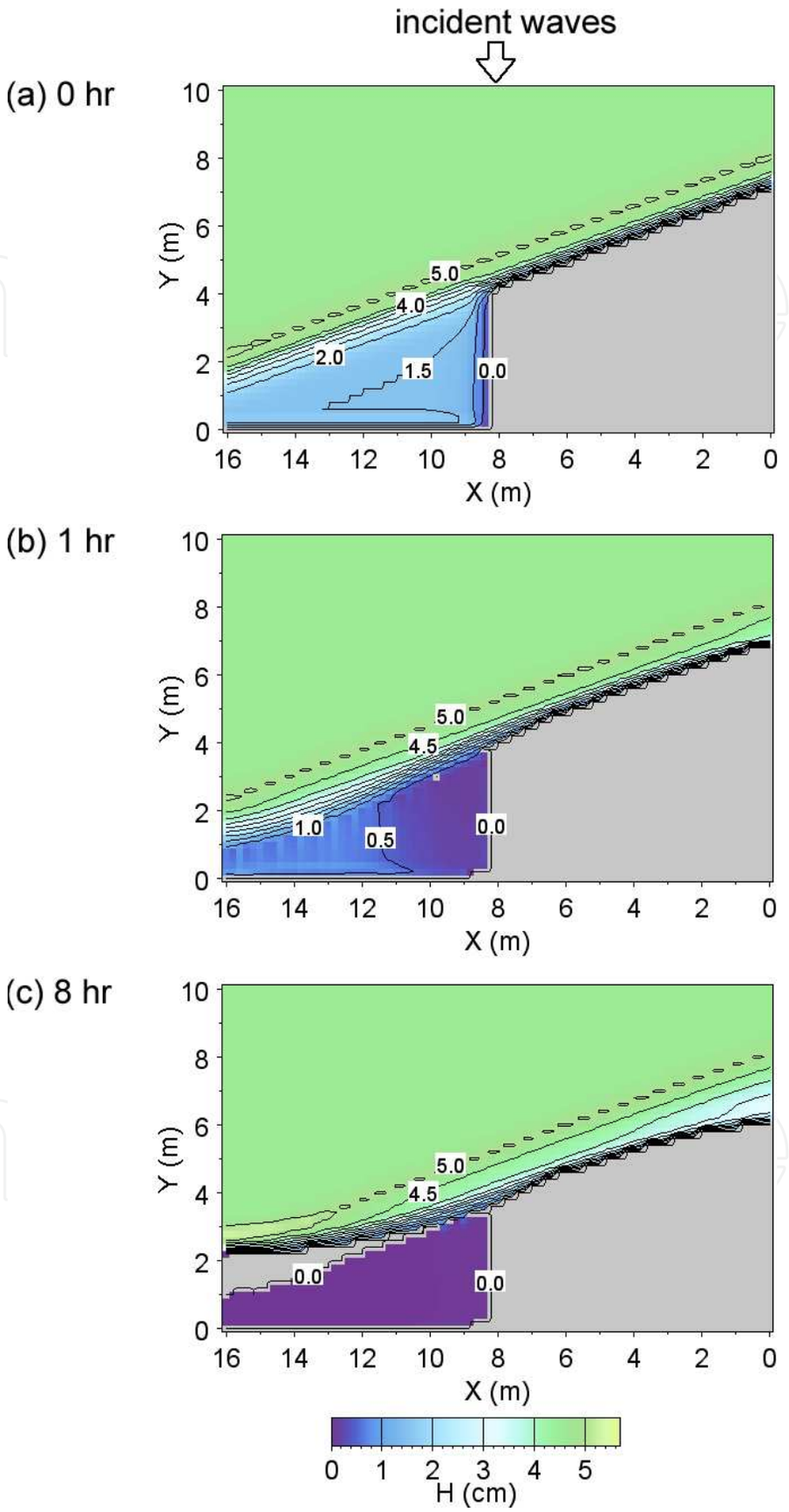

Figure 13. Changes in wave height (Case 1: flat shallow seabed).

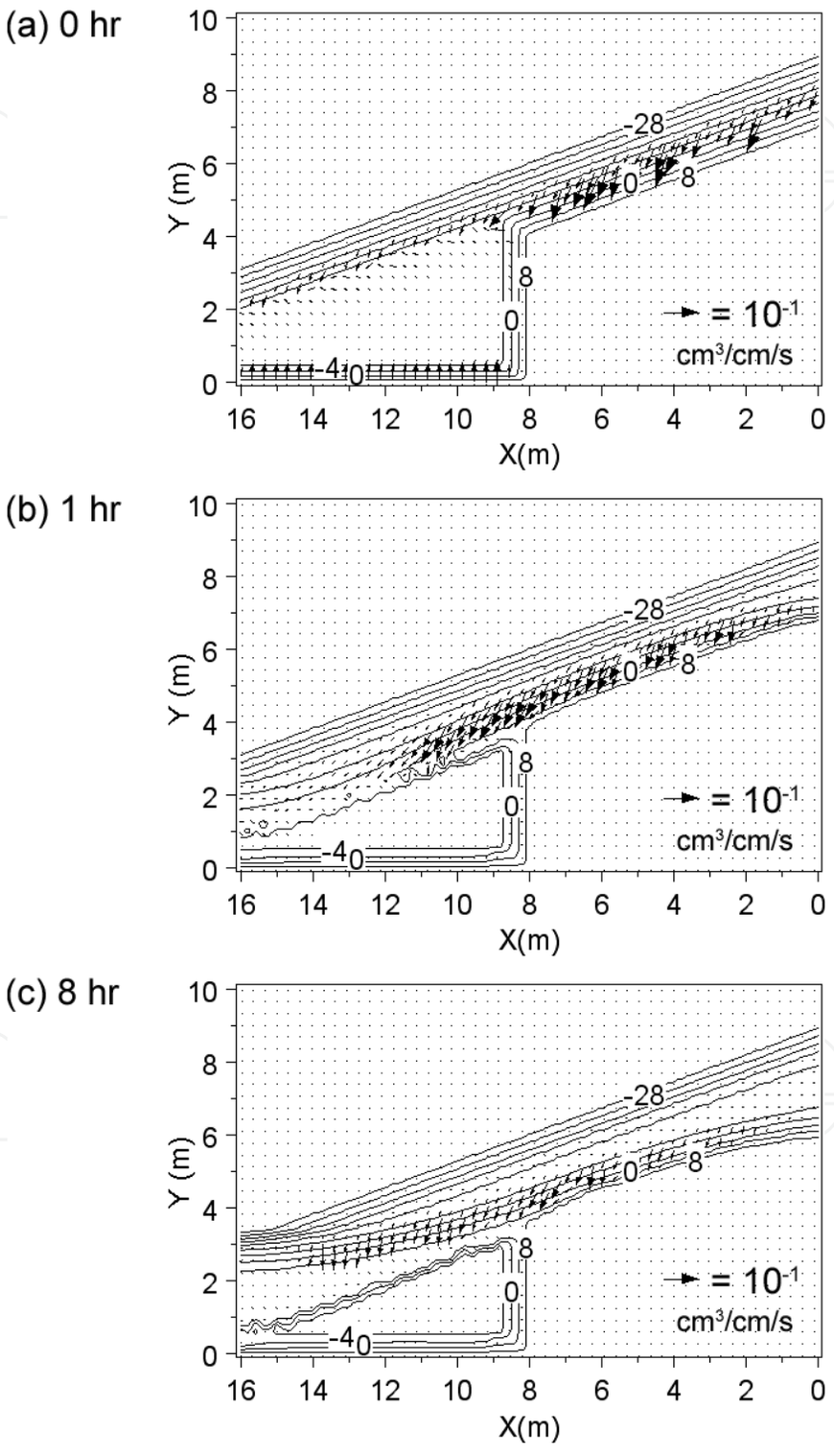

Figure 14. Sand transport flux (Case 1: flat shallow seabed).

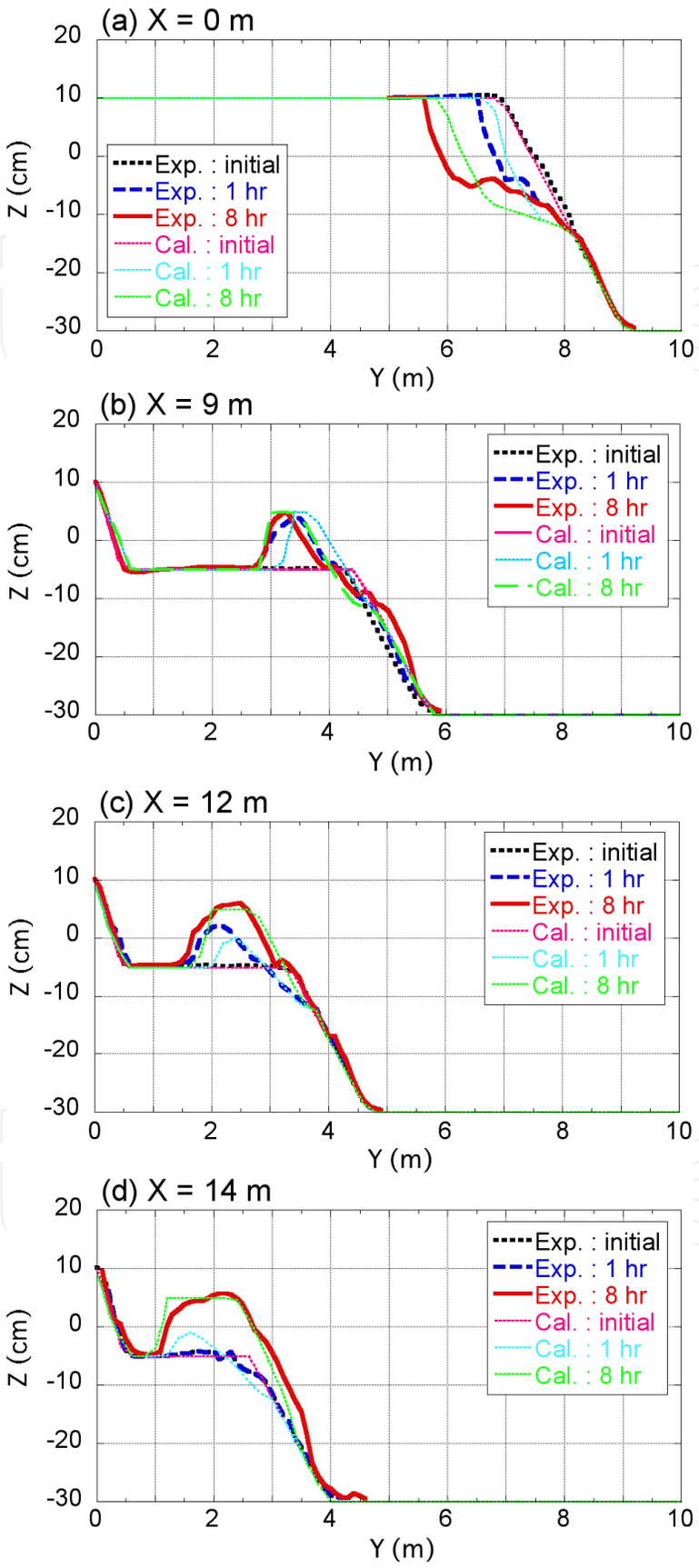

Figure 15. Changes in longitudinal profiles (Case 1: flat shallow seabed).

each other at the initial stage around the location with an abrupt change in the coastline orientation rapidly changed over time, causing sand deposition in the deep zone and the formation of a cuspate foreland after 0.5 hr. After 1 hr, the shoreline protruded further and a neck in the contour had formed downcoast of the sand deposition zone of the cuspate foreland. The size of this neck increased with time, and a sand spit that enclosed a shallow sea inside the neck had formed after 2 hr. This morphology is very similar to that of Miho Peninsula, formed by the extension of a sand spit, and Miho Bay in Shizuoka Prefecture (Uda & Yamamoto, 1994). Because of the continuous sand supply from upcoast, the sand spit elongated and the tip became connected to the downcoast shoreline. As a result, the shallow sea located inside the neck had formed a pond after 4 hr. After 8 hr, a steep slope had formed along the shoreline of the cuspate foreland owing to the continuous sand deposition in the deeper zone, whereas a wave base with a gentle slope had formed on the coast from which sand was supplied.

Figures 17(a)-17(f) show bird's-eye view of the development of a cuspate foreland on a steep coast. Although sand transported from upcoast was deposited on the steep seabed, the deposition of sand started near the location with an abrupt change in the coastline orientation, forming a neck in the contours, as shown in Figs. 17(a) and 17(b). This neck moved landward with time, and finally a sandy beach with a flat surface and a steep slope offshore of the shoreline had formed after 8 hr.

5.2.2. Changes in wave field

Figures 18(a)-18(c) show the distributions of the calculated wave height after wave generation for 0, 1 and 8 hr. At the initial stage, the longshore change in the wave height is large near the location with an abrupt change in the coastline orientation. Although a semicircular cuspate foreland developed until 1 hr, a marked decay in the wave height occurred over the short distance along the protruding shoreline, because the wave height was extremely low behind the protruded shoreline. The change in longshore sand transport due to this decay in wave height was successfully taken into account by the additional term given by Ozasa & Brampton (1980). The spatial change in longshore sand transport is large in this area because of the abrupt decrease in wave height, meaning that sand was rapidly deposited. However, after 8 hr, the area where the wave height abruptly decreased had disappeared and the wave height was smoothly distributed alongshore.

5.2.3. Sand transport flux

Figure 19 shows the sand transport flux after wave generation for 0, 1 and 8 hr. Although the sand transport flux was initially large to the right of X = 8 m, which is the sand supply area, as in Case 1, after 1 hr the area with a large sand transport flux had moved leftward with the elongation of the sand spit. Moreover, the sand transport flux was reduced because the angle between the direction normal to the contour lines and the direction of incident waves decreased near the right boundary. After 8 hr, the sand spit had reached the left boundary, and the absolute value of sand transport flux decreased because the angle

between the direction normal to the contour lines and the wave incidence direction had been reduced near both boundaries.

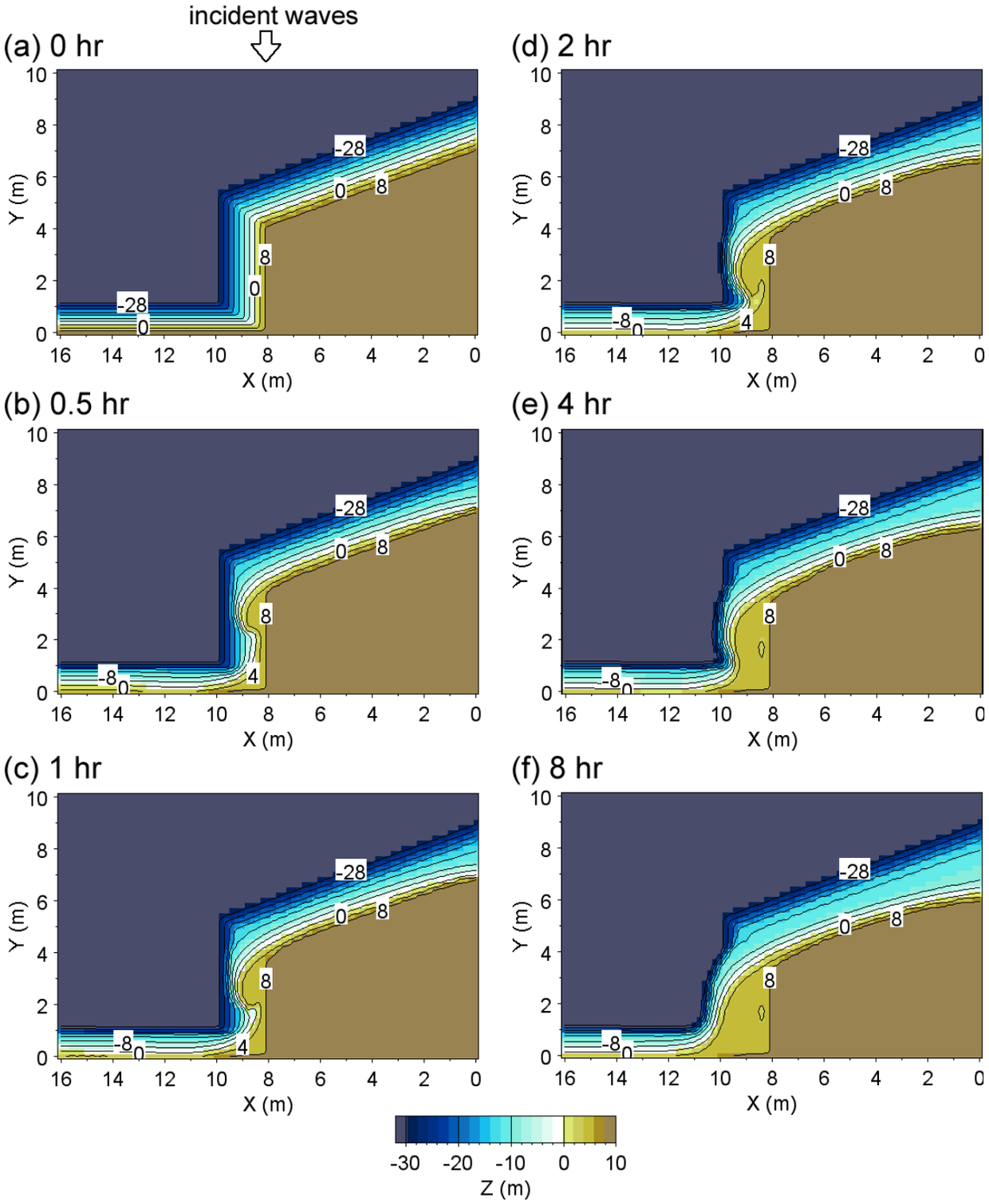

Figure 16. Predicted results for development of cuspate foreland on a coast with abrupt change in coastline orientation (Case 2: steep slope and deep seabed).

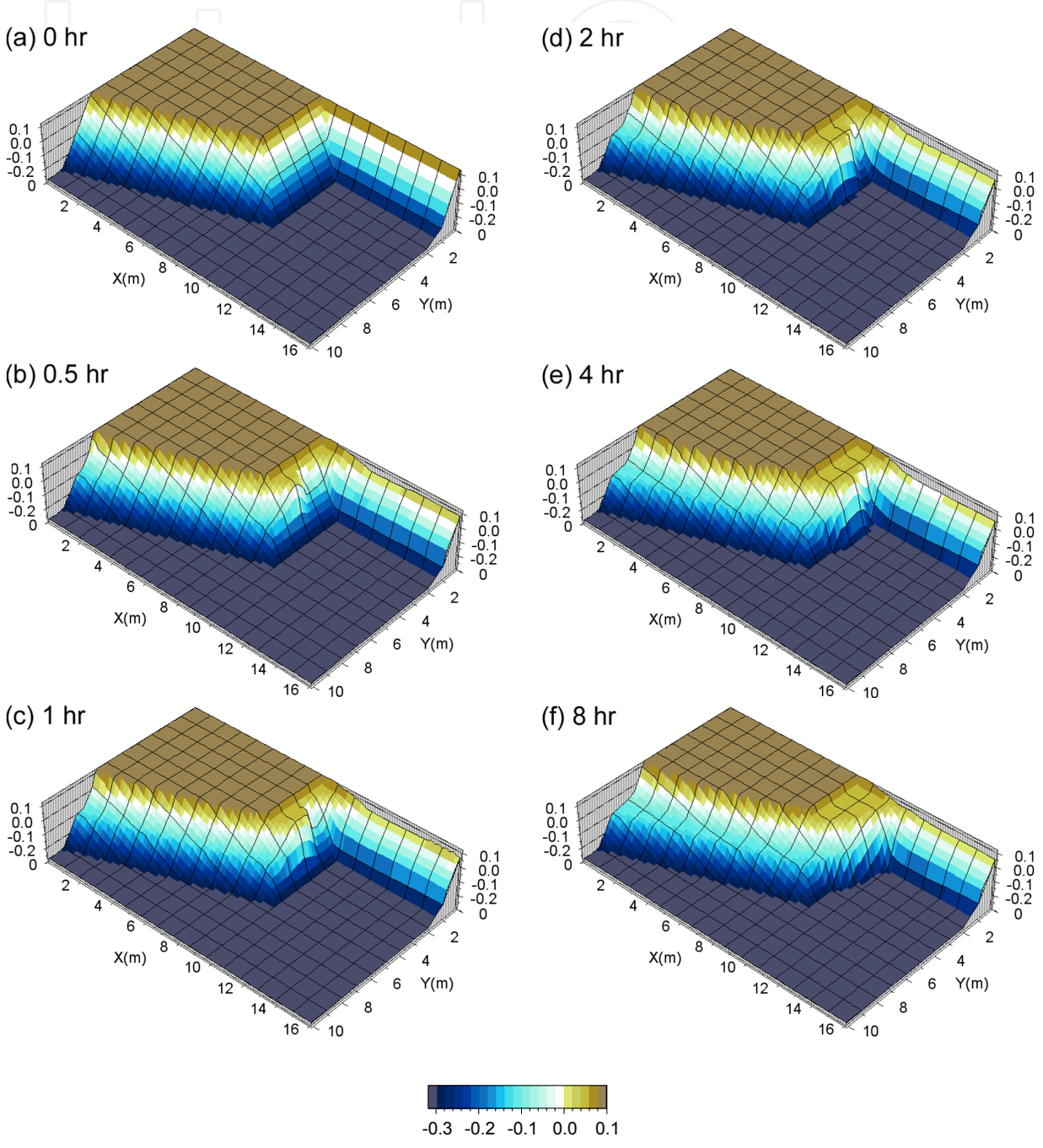

Figure 17. Bird's-eye view of topographic changes (Case 2: steep slope and deep seabed).

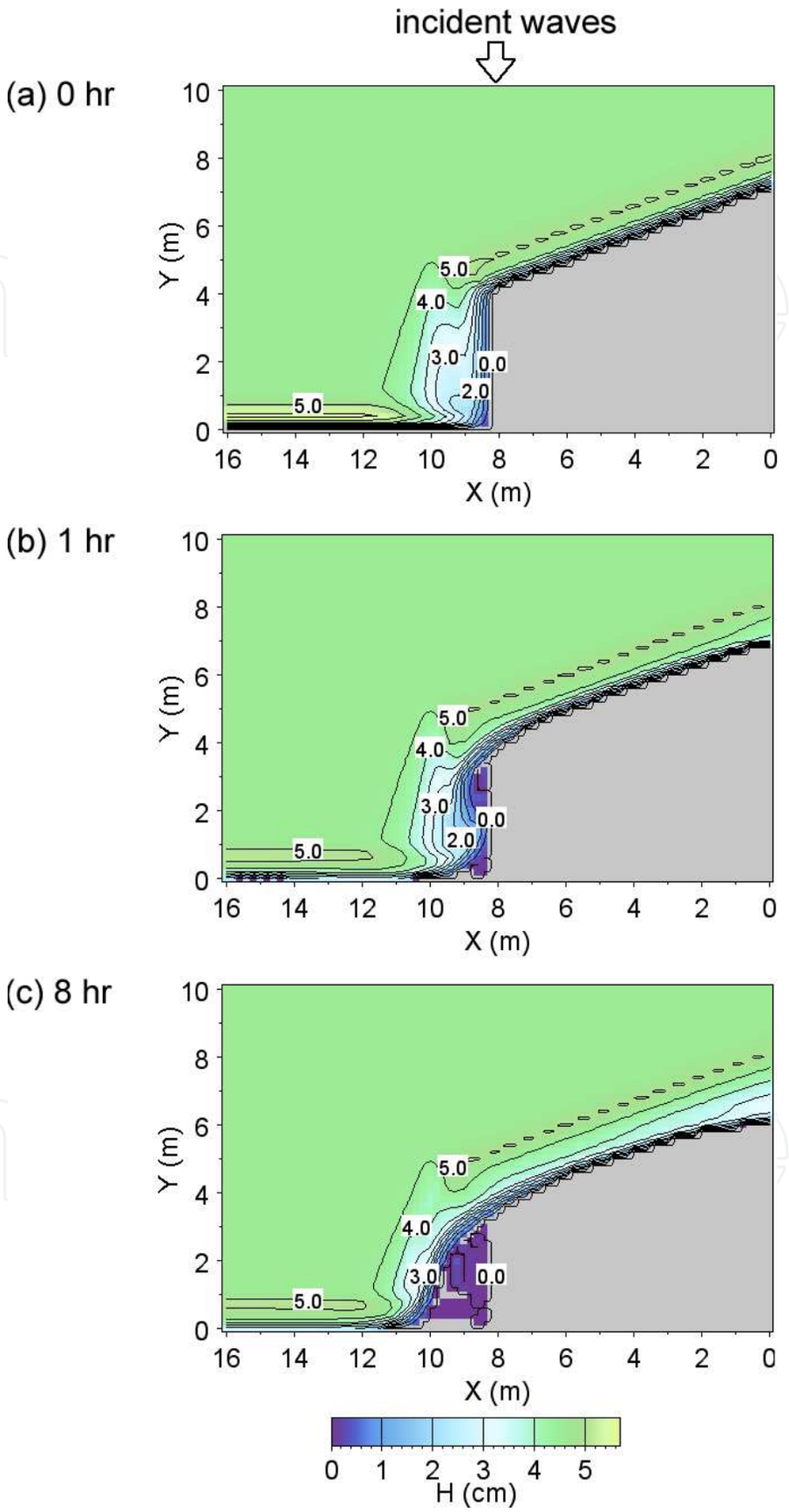

Figure 18. Changes in wave height (Case 2: steep slope and deep seabed).

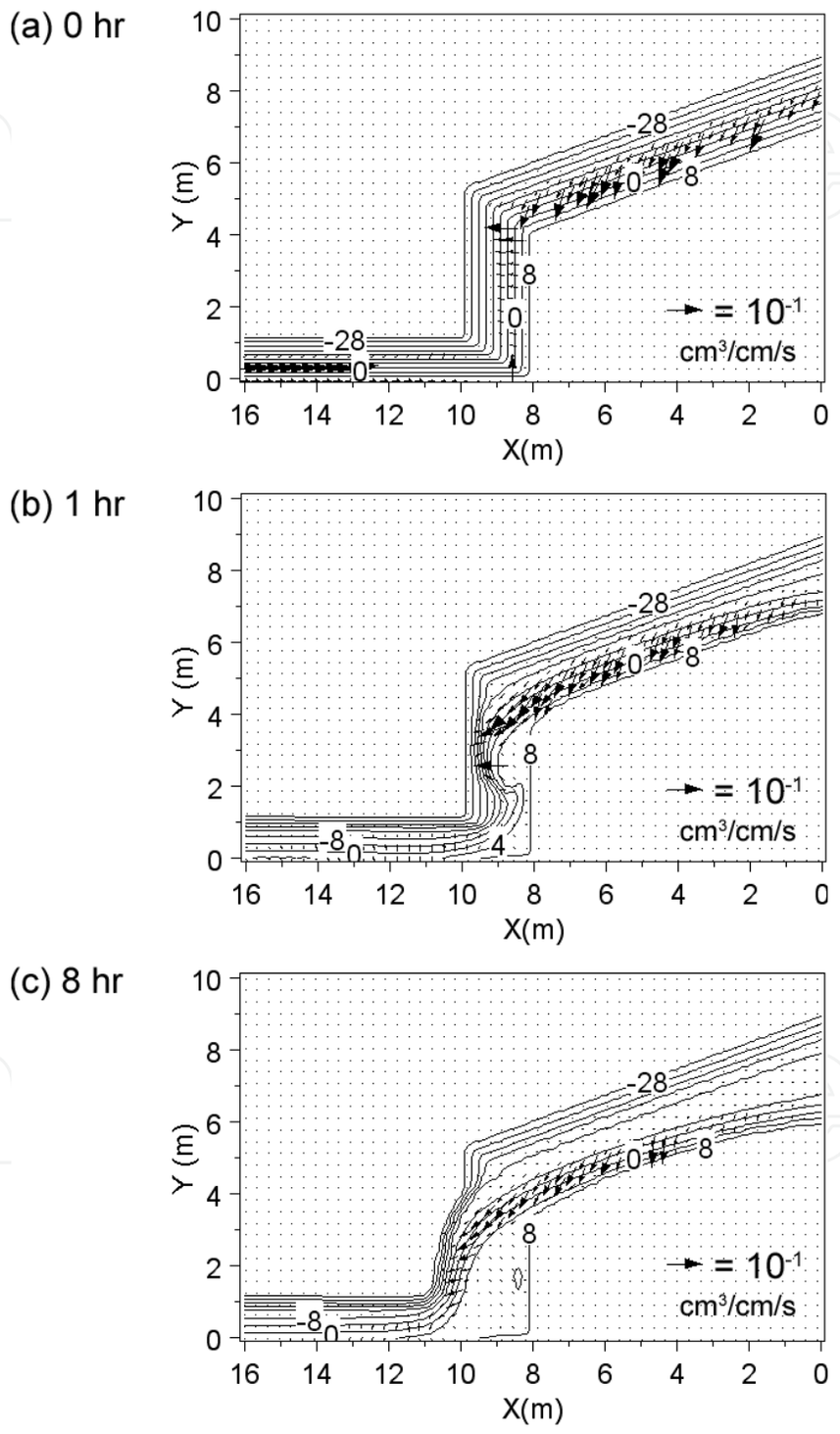

Figure 19. Sand transport flux (Case 2: steep slope and deep seabed).

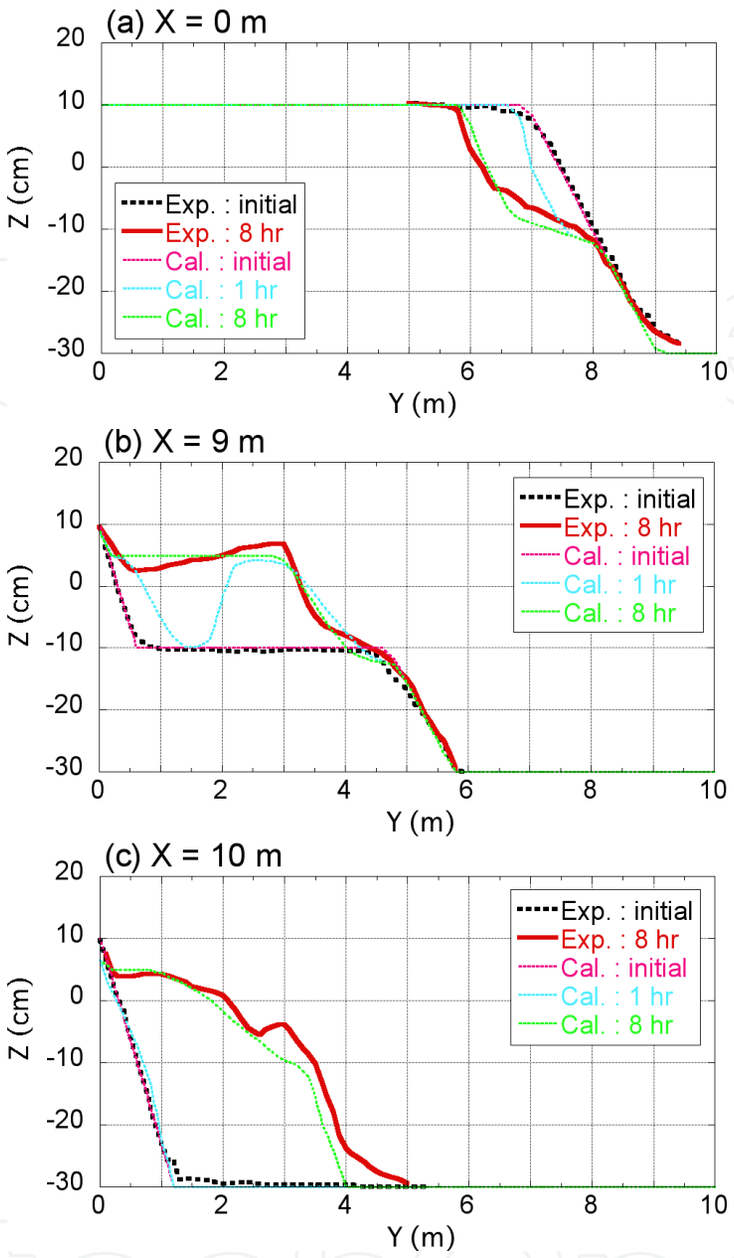

Figure 20. Changes in longitudinal profiles (Case 2: steep slope and deep seabed).

5.2.4. Changes in longitudinal profiles

Figures 20(a)-20(c) show the experimental and predicted changes in longitudinal profiles along transect X = 0 m located at the right boundary, transect X = 9 m near the location where the coastline orientation abruptly changes, and transect X = 10 m, respectively. Along transect X = 0 m, the parallel recession of the cross section is accurately reproduced in the calculation, as shown in Fig. 20(a). Along transect X = 9 m, a slope that slightly inclined landward had formed in the experiment after 8 hr, whereas a flat surface was predicted in the calculation. With the exception of these points, the experimental and predicted results are in good agreement, as shown in Fig. 20(b). The experimental and calculated results are also in good agreement along transect X = 10 m, as shown in Fig. 20(c).

6. Simulation of formation of slender sand bar on Kutsuo coast

To model the accumulation of sand on the tidal flat due to wave action and the formation of a slender sand bar, a point source in a single mesh (5 m×5 m) was assumed. The intensity of the point source was determined by trial and error, and it was set to 3.75×10^4 m^3/yr at the point (x, y) = (200 m, 0 m). In addition, an upper limit of 0.5 m was assumed as the elevation of the sandy island. When the elevation of the island reached this height during the calculation, the wave energy was set to 0.

Given the simplified initial topography and the conditions of the annual energy-mean waves of the Kutsuo coast (significant wave height H_i of 0.4 m and wave period T of 4 s), and assuming wave incidence from the direction normal to the coastline, the beach changes were predicted. The depth of closure was given by $h_c = 2.5H$ (H: wave height at a local point). The water depth of the initial bottom of the tidal flat was assumed to be 2 m. This initial flat bottom was assumed to be a solid bed, and a sandy beach with a slope of 1/10 was set at the landward end of the flat bottom. The berm height was assumed to be 0.5 m, and angles of the equilibrium slope and repose slope were set as 1/10 and 1/2, respectively. The calculation domain was divided by $\Delta x = \Delta y = 5$ m intervals in the cross-shore and longshore directions, respectively, and a calculation for up to 5000 hr (5×10^4 steps) was carried out using time intervals of $\Delta t = 0.1$ hr. Table 2 shows the calculation conditions.

6.1. Bathymetric changes

Figure 21 shows the calculation results obtained after every 10^4 steps. Initially, only a flat bottom extended offshore of the sandy beach with a straight shoreline. The solid circle in Fig. 21(a) shows the location of the sand source, and a sandy beach with a slope of 1/10 extended along the marginal line between the tidal flat and the land, as observed on the Kutsuo coast. Owing to the wave action under these conditions, a slender submerged sand bar started to form after 10^4 steps, as shown in Fig. 21(b), as a result of the deposition of sand supplied from the sand source. The landward end of the slender sand bar was sharp and similar to a comet tail formed on the lee of an island. On the other side of the slender sand bar, longshore sand transport toward the lee of the slender sand bar was induced from the nearby coast, resulting in the formation of a cuspate foreland because of the wave-sheltering effect of the sand bar. After 2×10^4 steps, the submerged sand bar had become a sandy island because of its continuous development (Fig. 21(c)). After 2×10^4 steps, the cuspate foreland behind the sandy island was more developed than that after 10^4 steps. The beach width in the zone between x = 50 and 100 m was very small and a neck was formed. After 3×10^4 steps, the widths of the sandy island and the neck behind the island had increased, and sand that had originally been supplied from the offshore point source had reached the beach, resulting in the connection of the sandy island to the beach (Fig. 21(d)). Finally, the island developed a spoonlike shape with the shoreline of a tombolo connected to the slender island.

The development of the sandy island continued up to 5×10^4 steps, and the widths of the sandy island and the neck between the island and the tombolo continued to increase (Figs. 21(e) and 21(f)). The numerical results for the development of a slender sand bar and the

resultant sandy island successfully explain the results observed on the Kutsuo coast, as shown in Fig. 3, and the fact that the slender sand bar has a neck near the landward end, as shown in Figs. 8-10.

Figures 22(a)-22(f) show bird's-eye view of the development of a slender sand bar developed on a flat seabed. Sand supplied from a sand source at (x, y) = (200 m, 0 m) was deposited to form an island with the gradual shoreward movement of sand. After 2×10^4 steps, a slender island connected to the land extended with the formation of a tombolo because of the wave-sheltering effect of the island itself. Because of the continuous supply of sand, the width of the island increased and the scale of the tombolo increased with increasing number of steps. The final configuration of the slender bar was very similar to that observed on the Kutsuo coast, as shown in Fig. 9.

Wave conditions	Incident waves: H_I = 0.4 m, T = 3 s, wave direction θ_I = 0°, normal to initial shoreline
Tide condition	H.W.L. = +2.0 m
Berm height	h_R = 0.5 m
Depth of closure	h_c = 2.5H (H: wave height)
Equilibrium slope	tanβ_e = 1/10
Angle of repose slope	tanβ_g = 1/2
Coefficients of sand transport	Coefficient of longshore sand transport K_s = 0.05 Coefficient of Ozasa & Brampton (1980) term K_2 = 1.62 K_s Coefficient of cross-shore sand transport K_n = 0.2 K_s
Mesh size	Δx = Δy = 5 m
Time intervals	Δt = 0.1 hr
Duration of calculation	5000 hr (5×10^4 steps)
Boundary conditions	Shoreward and landward ends: q_x = 0, left and right boundaries: q_y = 0
Calculation of wave field	Energy balance equation (Mase, 2001) •Term of wave dissipation due to wave breaking: Dally et al. (1984) model •Wave spectrum of incident waves: directional wave spectrum density obtained by Goda (1985) •Total number of frequency components N_F = 1 and number of directional subdivisions N_θ = 8 •Directional spreading parameter S_{max} = 10 •Coefficient of wave breaking K = 0.17 and Γ = 0.3 •Imaginary depth between minimum depth h_0 and berm height h_R:h_0 = 0.5 m •Wave energy = 0 where $Z \geq h_R$ •Lower limit of h in term of wave decay due to breaking: 0.2 m
Remark	Point source in single mesh (3.75×10^4 m^3/yr)

Table 2. Calculation conditions.

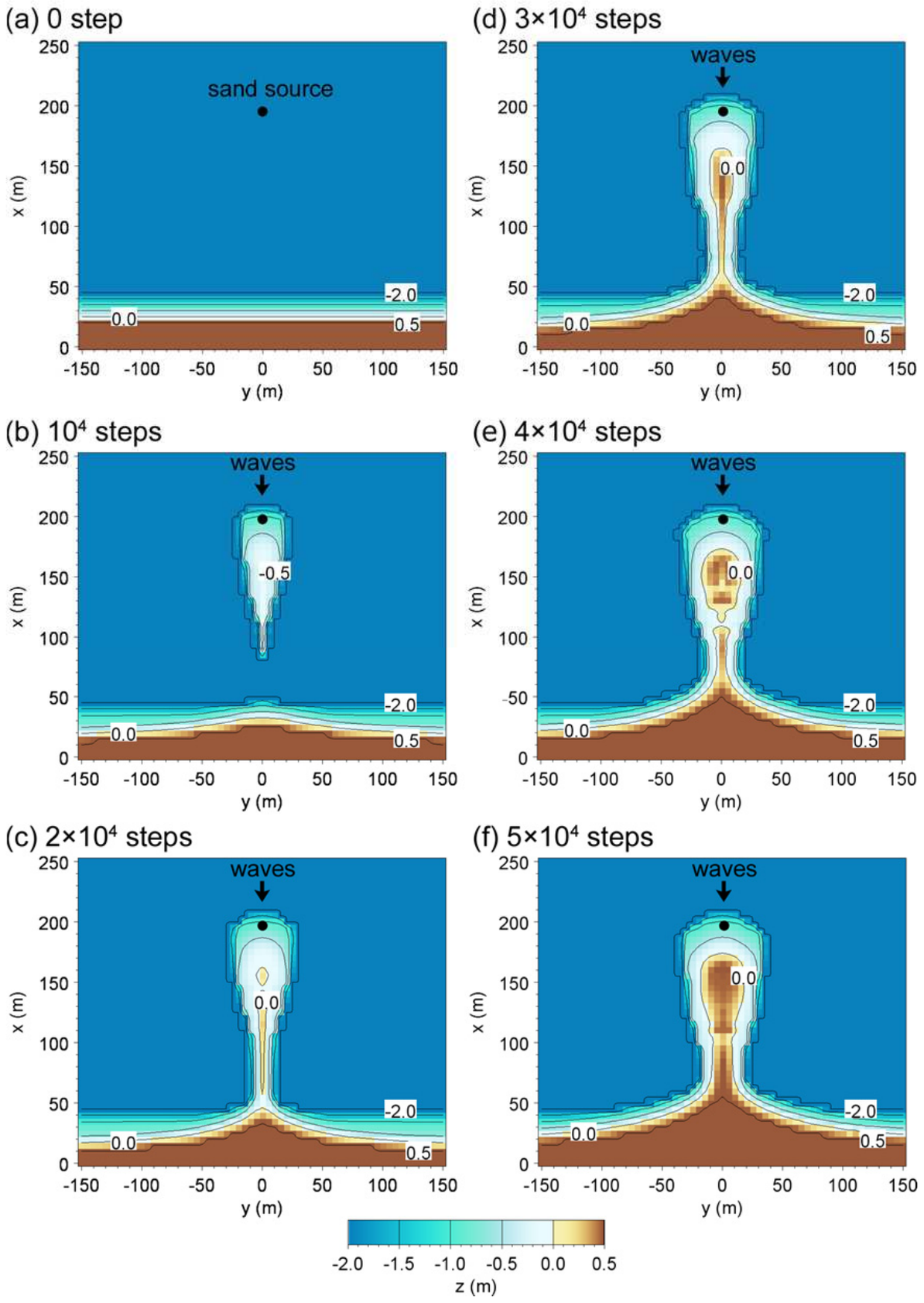

Figure 21. Calculation results observed after every 10^4 steps.

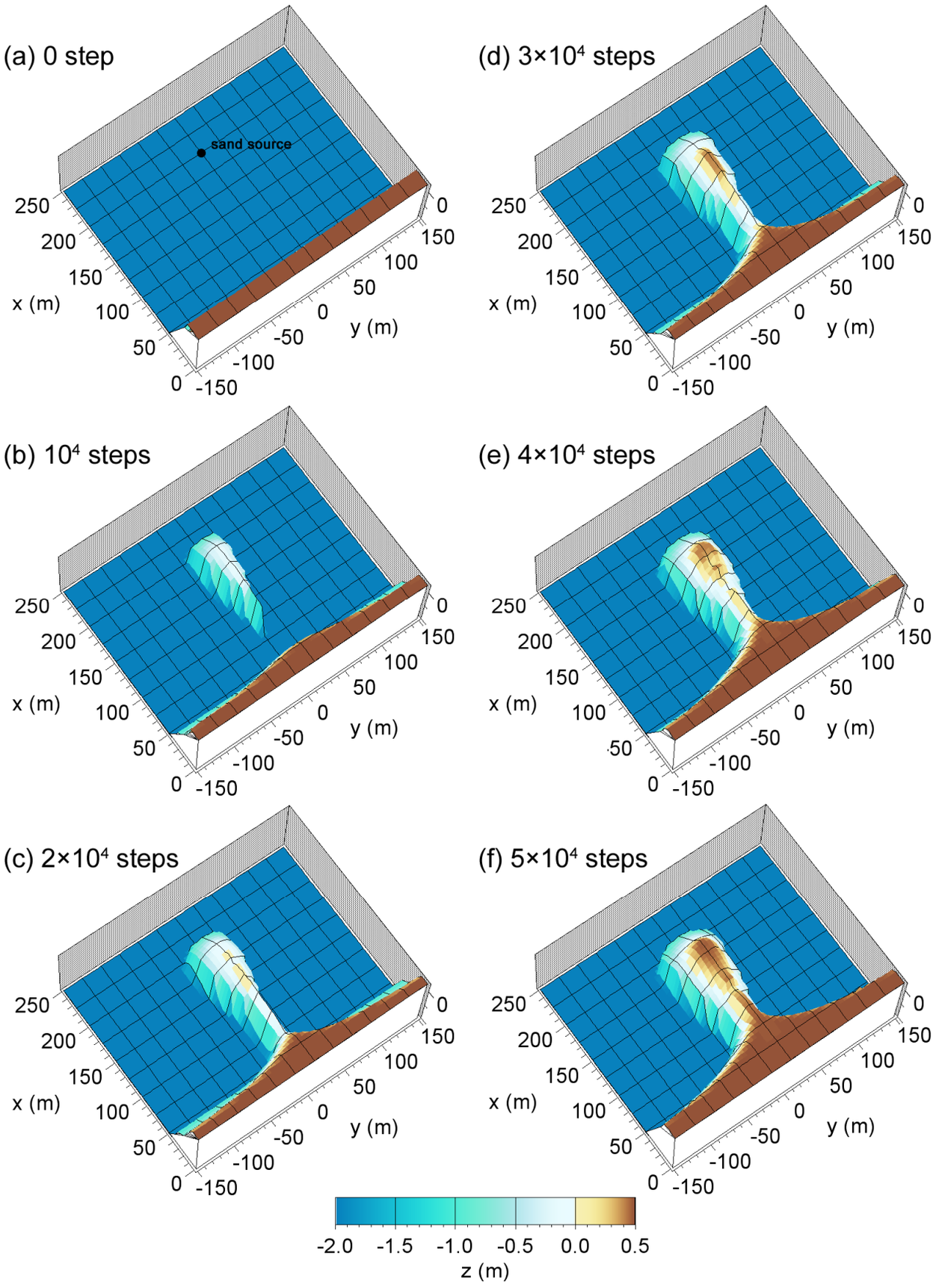

Figure 22. Bird's-eye view of topographic changes.

6.2. Changes in longitudinal and transverse profiles

Figure 23 shows the changes in the longitudinal profile along transect y = 0 m, which passes through the center of the slender sandy island, as shown in Fig. 21(f). Because the development of the sandy island along this transect was very rapid, the results obtained after not only 1 ×10^4 steps but also 5×10^3 and 1.5×10^4 steps are also shown. Although the sand bar gradually extended landward, the wave height along the side slopes of the sand bar (or the resultant sandy island) was reduced owing to the wave-sheltering effect induced by the sand bar itself, resulting in a decrease in the depth of closure along the side slope. For example, a steep slope with an angle of repose of 1/2 had formed in the zone deeper than Z = -0.3 m after 1×10^4 steps. The elevation of the beach connecting the land and the sandy island increased to reach the berm height of h_R = 0.5 m.

Figure 24 shows the changes in the cross section along transect x = 100 m, which passes through the neck of the slender sandy island, and transect x = 50 m near the boundary between the sandy beach and the tidal flat under the initial conditions, as shown in Fig. 21(f). After 10^4 steps, an island with a sharp top and a side slope with a steep angle of repose on both sides of the island had formed along transect x = 100 m. The increase in the width of the sandy beach over time was slow. In contrast, because of the increase in the wave-sheltering effect owing to the development of the sandy island, the cuspate foreland was more developed along transect x = 50 m than along transect x = 100 m, and its width increased over time.

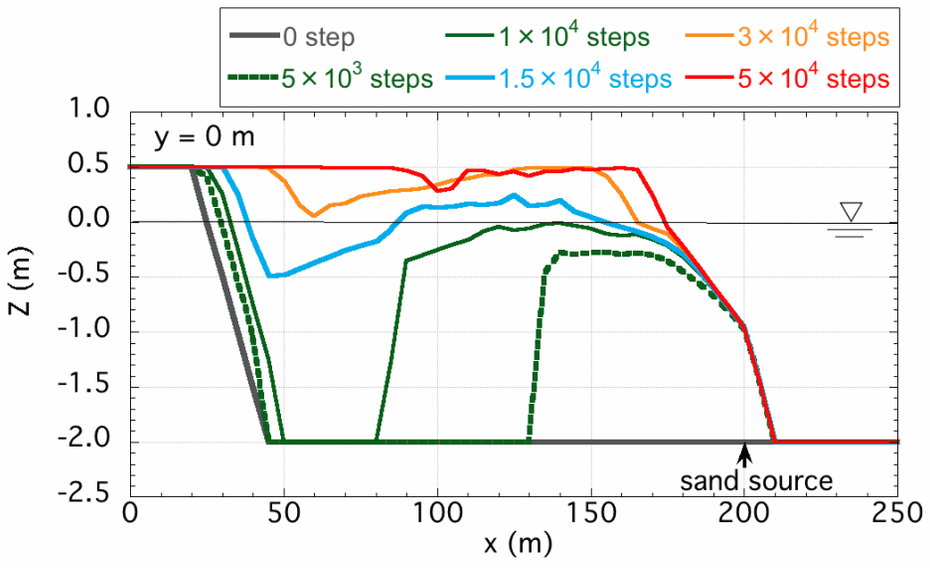

Figure 23. Changes in longitudinal profile along transect y = 0 m passing through center of slender sandy island.

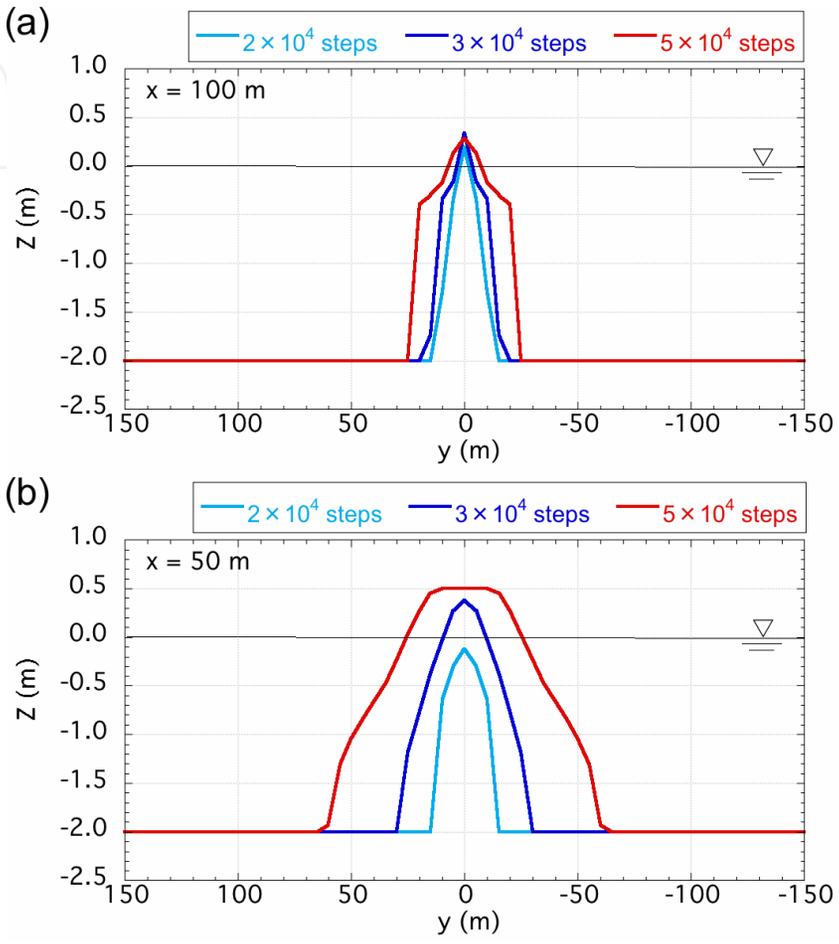

Figure 24. Changes in cross section along transect x = 100 m passing through neck of slender sandy island and transect x = 50 m near boundary between sandy beach and tidal flat.

6.3. Wave height and direction

The wave fields corresponding to the beach changes are shown in Fig. 25. The wave height on the tidal flat was initially uniform (0 step) and uniform wave decay due to wave breaking occurred on the sandy beach extending between the land and the tidal flat. After 1×10^4 steps, a submerged sand bar had been formed by the accumulation of sand supplied from a point source. This sand bar induced a change in the wave field; the wave height was reduced along the side slope of the slender sand bar, and oblique wave incidence occurred on both sides of the sand bar owing to wave diffraction by the sand bar itself. This oblique

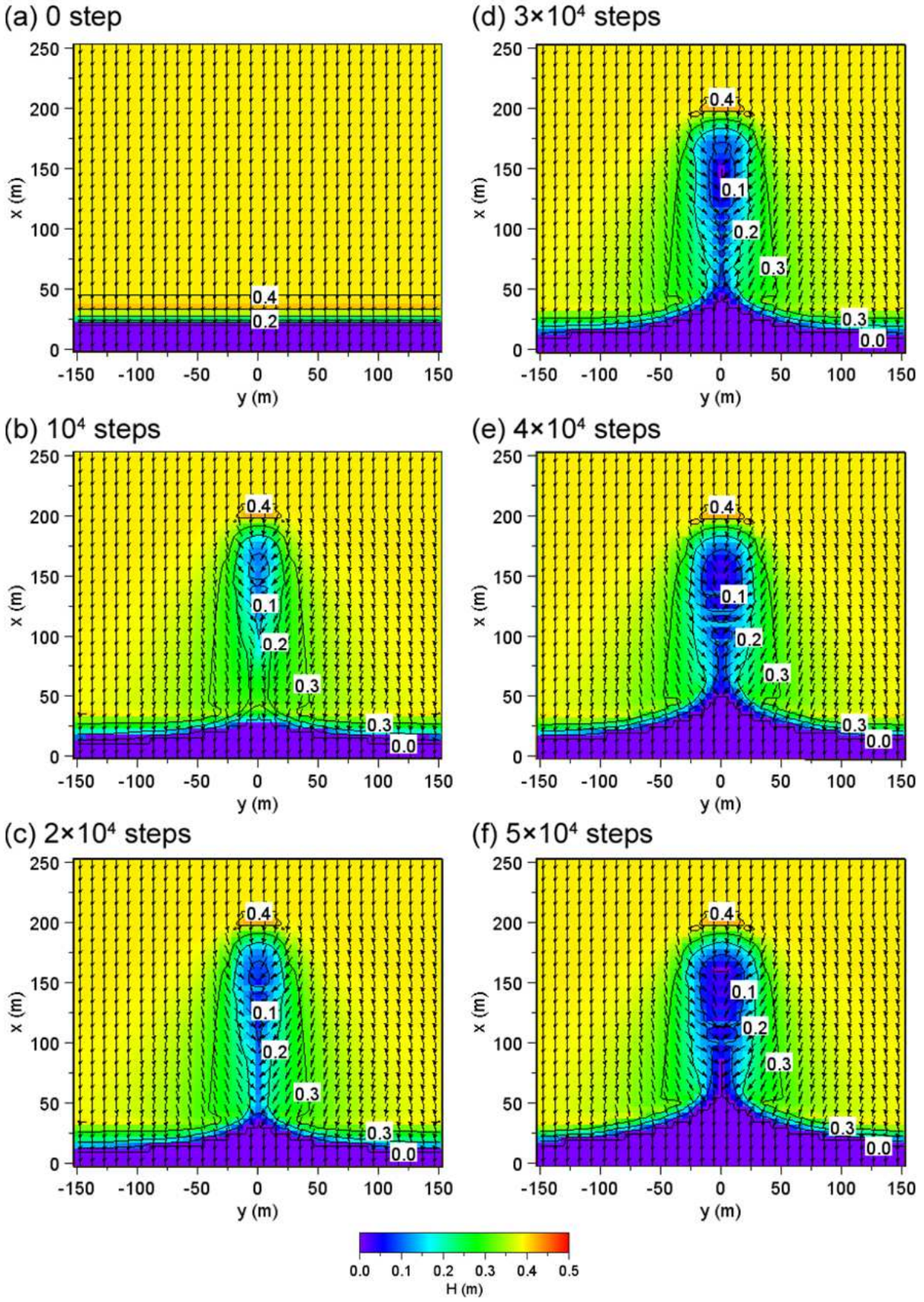

Figure 25. Wave fields corresponding to beach changes.

wave incidence caused shoreward sand transport flux along the contours of the sand bar. On the other hand, on the lee of the submerged sand bar, the wave height was reduced, similarly to in the case of a detached breakwater, inducing longshore sand transport toward the lee of the sand bar from outside the wave-shelter zone. After 2×10^4 steps, as a result of the landward extension of the slender sand bar and the decrease in water depth, wave breaking occurred there, causing a marked reduction in wave height. At the same time, the oblique wave incidence continued in this area and landward sand transport from the island to the land continuously occurred. After 4×10^4 and 5×10^4 steps, the same beach changes as those until 2×10^4 steps continued.

7. Conclusions

The BG model was applied to predict the development of a sand spit on a flat shallow seabed and the formation of a cuspate foreland on coasts with an abrupt change in the shoreline orientation. The results of the model were validated by comparison with the experimental results obtained by Uda & Yamamoto (1992). The predicted and measured results were in good agreement. As another type of beach change due to waves on a coast with a shallow flat seabed, the shoreward transport of sand originally supplied from the offshore zone of a tidal flat, forming a slender sand bar, and the landward deposition of such sand were observed on the Kutsuo coast, which has a very wide tidal flat and faces the Suo-nada Sea, part of the Seto Inland Sea. We investigated these phenomena by field observations and then performed a numerical simulation using the BG model. The observed results were successfully explained by the results of the numerical simulation. Although the BG model has been used to predict the development of river mouth bars, a single sand spit and a bay barrier (Serizawa et al., 2009b, 2009a; Uda & Serizawa, 2011), another application was demonstrated in the present study.

Author details

Takaaki Uda
Public Works Research Center, Taito, Tokyo

Masumi Serizawa and Shiho Miyahara
Coastal Engineering Laboratory Co., Ltd., Shinjuku, Tokyo

8. References

Ashton, A.; Murray, A. B. & Arnault, O. (2001). Formation of coastline features by large-scale instabilities induced by high angle waves, *Nature*, Vol. 14, No. 6861, (November 2001), pp. 296-300, ISSN 0028-0836

Bagnold, R. A. (1963). Mechanics of Marine Sedimentation, In: *The Sea*, Hill, M. N. (editor), Vol. 3, pp. 507-528, Wiley, ISBN 978-0674017306, New York

Bailard, J. A. & Inman, D. L. (1981). An energetics bedload model for a plane sloping beach: Local transport, *J. Geophys. Res*., Vol. 86, C3, pp. 2035-2043

Dally, W. R.; Dean, R. G. & Dalrymple, R. A. (1984). A model for breaker decay on beaches, *Proc. 19th ICCE*, pp. 82-97,Houston, Texas, USA, September 1984

Goda, Y. (1985). *Random Seas and Design of Maritime Structures*, University of Tokyo Press, ISBN 978-9810232566, Tokyo

Inman, D. L. & Bagnold, R. A. (1963). Littoral Processes, In: *The Sea*, M. N. Hill (editor), Vol. 3, pp. 529-533, Wiley, ISBN 978-0674017306, New York

Mase, H. (2001). Multidirectional random wave transformation model based on energy balance equation, *Coastal Eng. J*., JSCE, Vol. 43, No. 4, (December 2001),pp. 317-337.

Ozasa, H. & Brampton, A. H. (1980). Model for predicting the shoreline evolution of beaches backed by seawalls, *Coastal Eng*., Vol. 4, pp. 47-64

Serizawa, M.; Uda, T.; San-nami, T. & Furuike, K. (2006). Three-dimensional model for predicting beach changes based on Bagnold's concept, *Proc. 30th ICCE*, pp. 3155-3167, ISBN 978-981-270-636-2, San Diego, California, USA, September 2006

Serizawa, M.; Uda, T.; San-nami, T.; Furuike, K. & Ishikawa, T. (2009a). Prediction of topographic changes of sand spit using BG model, *J. Coastal Res*., SI 56, pp. 1060-1064

Serizawa, M.; Uda, T.; San-nami, T.; Furuike, K. & Ishikawa, T. (2009b). Model for predicting recovery of a river mouth bar after flood using BG model, *Asian and Pacific Coasts 2009*, *Proc. 5th International Conf*., Vol. 3, pp. 96-102, Singapore, October 2009

Serizawa, M. & Uda, T. (2011). Prediction of formation of sand spit on coast with sudden change in coastline using improved BG model, *Coastal Sediments '11*, pp. 1907-1919, Miami, Florida, USA, May 2011

Serizawa, M.; Uda, T. & Miyahara, S. (2011). Model for predicting formation of slender sand bar due to shoreward sand transport on shallow tidal flat, *Asian and Pacific Coasts 2011, Proc. 6th International Conf*., pp. 1477-1484, ISBN 978-981-4366-48-9, Hong Kong, December 2011

Uda, T. & Kawano, S. (1996). Development of a predictive model of contour line change due to waves, *Proc. JSCE*, No. 539/ II -35, pp. 121-139. (in Japanese)

Shimizu, T.; Kumagai, T. & Watanabe, A. (1996). Improved 3-D beach evolution model coupled with the shoreline model (3D-SHORE), *Proc. 25th ICCE*, pp. 2843-2856, Orlando, Florida, USA, September 1996

Uda, T. & Yamamoto, K. (1992). On relationship between seabed topography and formation of spit, *Trans. Jpn. Geomor. Union*, Vol. 13, pp. 141-157 (in Japanese)

Uda, T. & Yamamoto, K. (1994). Beach erosion around a sand spit-an example of Mihono-Matsubara sand spit-, *Proc. 24th ICCE*, pp. 2726-2740, Kobe, Japan, October 1994

Uda, T. & Serizawa, M. (2010). Model for predicting topographic changes on coast composed of sand of mixed grain size and its applications (Chap. 16), In: *Numerical simulations-examples and applications in computational fluid dynamics*,Angermann, L. (Ed.), pp. 327-358, INTECH,http://www.intechopen.com/articles/show/title/model-for-

predicting-opographic-changes-on-coast-composed-of-sand-of-mixed-grain-size-and-its-appli

Uda, T. & Serizawa, M. (2011). Model for predicting formation of bay barrier in flat shallow sea, *Coastal Sediments '11*, pp. 1176-1189, Miami, Florida, USA, May 2011

Watanabe, S.; Serizawa, M. & Uda, T. (2004). Predictive model of formation of a sand spit, *Proc. 29th ICCE*, pp. 2061-2073, ISBN 981-256-298-2, Lisbon, Portugal, September 2004

IntechOpen